Research Article | Vol. 29, No. 6 / 15 March 2021 / Optics Express 8041

Optics EXPRESS

Curvature effect on surface topography and uniform scallop height control in normal grinding of optical curved surface considering wheel vibration

SHANSHAN CHEN,[1] SHUMING YANG,[1,5] ZHIRONG LIAO,[2,6] CHI FAI CHEUNG,[3] ZHUANGDE JIANG,[1] AND FEIHU ZHANG[4]

[1]School of Mechanical Engineering, Xi'an Jiaotong University, 28 Xianning West Road, Xi'an, Shaanxi, 710049, China
[2]Faculty of Engineering, University of Nottingham, NG7 2RD, UK
[3]State Key Laboratory of Ultraprecision Machining Technology, The Hong Kong Polytechnic University, Hung Hom, Kowloon, 999077, Hong Kong
[4]School of Mechatronics Engineering, Harbin Institute of Technology, Harbin, 150001, China
[5]shuming.yang@mail.xjtu.edu.cn
[6]Zhirong.Liao@nottingham.ac.uk

Abstract: High-precision optical components with complex shapes or microstructures have been extensively used in numerous fields such as biomedicine, energy and aerospace. In order to accurately achieve the specific functions of the components, the form accuracy and uniform surface quality need to reach an ever-high level. To achieve this, ultra-precision normal grinding is used for machining various types of complex optical surfaces. However, the intricate variation of the workpiece curvature and grinding wheel vibration gives rise to great challenges to obtain higher precision and uniform surface conditions. In this study, the influence of curvature on surface topography generation has been investigated and a novel model of scallop height has been developed for surface topography generation in the normal grinding of the curved surface. In addition, the relative influence of the curvature is analyzed experimentally, in which the micro-waviness generation as a consequence of the unbalanced vibration of the grinding wheel is modeled and validated by experiments. Finally, the micro sinusoidal array with the setting value for scallop height is achieved by controlling the feed speed, which is determined by the local curvature of surface profile. The results indicated that the curvature variation posed a significant effect on surface uniformity and the model is valid to achieve surface scallop height control in the normal grinding effectively.

1. Introduction

The development of advanced optics has dramatically increased the demand of various optical curved surfaces, such as aspheric [1], micro lens array [2,3] and even free-form surface [4–6]. The complex curved surfaces have become the key component in optical system due to their high imaging quality and simple system structure. Many types of freeform or aspheric optical elements with high-resolution are used in solar concentrators, lithography, azimuth lighting and collimator systems [7]. Nowadays high accuracy glass molding is a primary method to fabricate optic elements with the various complex structure, in which Tungsten Carbide is the most frequently used as a molding material due to good dimensional stability and wear resistance at the elevate temperature [8,9]. However, it is one of difficult-to-machine materials and the ultra-precision grinding is frequently adopted to machine this kind of material [10,11]. To achieve required functions of optical components accurately, high accuracy and uniform surface topography should be guaranteed in the machining [12–15]. Surface topography plays a vital

#418599 https://doi.org/10.1364/OE.418599
Journal © 2021 Received 4 Jan 2021; revised 12 Feb 2021; accepted 15 Feb 2021; published 1 Mar 2021

Optics EXPRESS

role in the optical functions, which formed by the engagement movement between the tool and workpiece [16]. Therefore, an accurate theoretical model for the surface topography generation is very essential to improve and control optical performance of machined parts [17,18]. However, in the grinding of intricate curved surface, the complicated curvature variation and frequent change of curvature center present great challenges to achieve high quality surface finish.

The surface topography generation process is normally highly related to the surface quality and it is governed by various technological parameters in the ultra-precision grinding, such as wheel properties and geometry, workpiece specifications and operation parameters [19,20]. The features of the machined surface mainly include geometric form error, roughness and waviness while the ground surface topography is mainly formed by the superposition of these three features. At present, most research work about surface generation in the grinding is focused on revealing the effect of technical parameters or wheel vibration on surface quality. Chuang and Tso [21] studied the influence of operation parameters on form accuracy and found that the form accuracy improved with the increasing tilted angle between the wheel and workpiece. Zhou and Xi [22] derived a popular model to predict surface topography generation by combining the random feature of abrasive grain and wheel wear conditions. Li et al. [23] developed a grinding force model based on the trajectory and distribution of abrasives grain, in which the statistical parameters of tip radius for abrasive grain were calculated based on the analysis of micro groves left by grains. Wu et al. [24] developed a model for surface topography formation and predicted the surface roughness by considering the random features of abrasive grain, such as protrusion height, grit size and location distribution. Li et al. [25] simulated the surface generation and evaluated surface roughness in the grinding by including random features of the radius and protrusion height of abrasive grains and it is found that the abrasive size is the dominate factor to determine the surface quality. Xiao et al. [26] analyzed the kinematic characteristics of abrasive grains and calculated the effect of each machining parameter on the surface roughness. Based on that, the relationship between the surface roughness and subsurface damage is established and found that the coupling effect (speed ratio) between the wheel and workpiece speed acts an important aspect in the evolution of surface quality and subsurface damage.

Chen et al. [27] established a model of grinding marks generation in machining of aspheric surface by considering the runout of the wheel. In their research, the pattern of the marks was investigated and a strategy to suppress the grinding marks was proposed. Wang et al. [28] systematically analyze the effect of machining variables and radical run out of the wheel on the surface generation. It is found that the ratio of wheel speed to workpiece speed posed a significant effect on the tilted angle and spatial period of the ground surface marks as well as surface scallop height. He et al. [29] developed a multifrequency vibration model for surface topography generation in turning operation and found that the surface roughness and form error were nonuniform over the entire machined surface at radial position of the workpiece. It is found that vibration amplitude has a remarkable impact on specular reflectivity and optimum machining parameters were proposed to minimize the vibration effect [30]. Chen et al. [31] investigated the effect of primary factors on surface quality and surface generation and found that vibration marks are the dominant features on the machined surface, which are arisen from the unbalanced wheel vibration. In addition, the phase shift effect of the tool vibration has also been investigated, which has a major influence on surface roughness and vibration mark geometry. Beaucamp et al. [32] developed an elastic grinding wheel to make the shape of contact area between the tool and workpiece changing with the workpiece curvature; however, the relationship between the curvature and surface generation is not revealed. Xu et al. [33] developed a surface generation algorithm in the grinding of spherical surface with a cup grinding wheel, in which the triangle grooves generated by abrasive grains and undeformed chip thickness were analyzed. In addition, the impact of grinding parameters and the number of wheel block on the surface roughness were also investigated respectively. However, the model is established based on the trajectory of the

Optics EXPRESS

abrasive grain on the workpiece surface and the effect of curvature on surface roughness and surface generation is not considered.

In the grinding of complex surface, tool path is a key element, which determines the surface quality and tolerance. Zhang et al. [34] designed a novel hybrid structure by combining the freeform and micro lens array to enhance luminous flux, in which the wheel tip is dressed as a V-shape and a tool path is designed along the part curvature. However, the influence of curvature on structure generation has not been considered. Yan and Fang [35] explored a novel normal grinding method in machining of freeform surface and developed a novel tool path control strategy by considering the tool pose and wheel geometry to avoid the translation of wheel errors onto the ground surface. Xie et al. [36] systematically investigated the influence of tool pose, self-dressing conditions, wheel geometry and protrusion height of the abrasive grain on tool interference and surface roughness in grinding of a F-theta freeform lens. Guo and Zhao [37] calculated the scallop height in normal grinding by considering the interference of adjacent pass of the grinding wheel. Lin et al. [38] developed a tool wear model by considering the variation of contact point between the cutting arc of the tool and workpiece in grinding of aspheric surface and relevant error compensation was conducted. Wan et al. [39] proposed a novel tool path strategy to adjust the contact area and tilted angle of the grinding wheel according to the limitation of figure tolerance. Wang et al. [40] developed a cutting force model by considering the operation parameters and contact region geometry between the grinding wheel and component, in which a tool path control method is presented to control the machining accuracy in the way of maintaining constant grinding force in the grinding of a large optical SiC mirror. He and Chen [41] presented a tool posture control method to keep the grinding strip width constant by considering the curve variation in machining of freeform surface. Chen et al. [42] studied the influence of curvature variation on the scallop height in the parallel grinding and investigated the geometrical relation between scallop height and curvature radius, in addition the surface matching algorithm is established to verify the model reliability of the surface generation. However, the relative effect of the curvature on surface generation is not conducted and the vibration effect posed a significant effect on the scallop height is not included in the model. It is found that there is the larger form error involved in parallel grinding of non-rotational symmetric surface in comparison with machining of rotational symmetric surface.

In grinding of complex optical surface, the curvature variation and constant change of curvature center are the major differences from the grinding of flat or spherical surface. Therefore, it is essential to look insight into the effect of curvature on the surface generation to enhance the capacity of surface uniformity control. In this research, the relative influence of curvature on the surface generation is evaluated in the normal grinding. In addition, the vibration marks generated on the workpiece surface with different radii are modeled. Based on that, a novel model of the scallop height is developed by considering the curvature and wheel vibration. Finally, the normal grinding experiment for the complex curved surface is conducted to verify the novel model.

2. Influence of curvature effect on vibration marks geometry

In our previous studies, it has been revealed that the grinding wheel is the largest error source for surface generation in machining of flat surface and proposed that the tool vibration resulted in appearance of micro-waviness on the machined surface, which can significantly affect the surface finish and tolerance [31,43]. This theory is also applicable in the ultra-precision grinding of curved surfaces, as shown in Fig. 1(a) and Fig. 1(b), whereby the relative vibration can result in the waviness in the curved surface generation. However, different from the grinding of flat surface, in machining of curved surface the variable center of curvature and curvature radius contribute to variable contact areas between the arc wheel with a nose radius and workpiece profile, which results in different scallop height generation (generated by cutting profile of wheel nose) on the machined surface. As shown in Fig. 1(c), the grinding wheel with an arc nose traverses the curved

Optics EXPRESS

surface profile, the interference of neighboring cutting path results in scallop height generation and the scallop height is different with respect to various curvature radius ($\Delta h_i \neq \Delta h_j \neq \Delta h_k$) under the same feed rate (S). In addition, the further increase for the scallop height due to the wheel vibration constantly changes at different curvatures ($\Delta Z_i \neq \Delta Z_j \neq \Delta Z_k$) under the same feed rate (S) and vibration amplitude ($\Delta A_i = \Delta A_j = \Delta A_k$), as shown in Fig. 1(c). It indicates that the curvature plays a critical role in surface generation in the normal grinding. Therefore, it is essential to study the curvature effect to achieve uniform surface quality in grinding of curved surface.

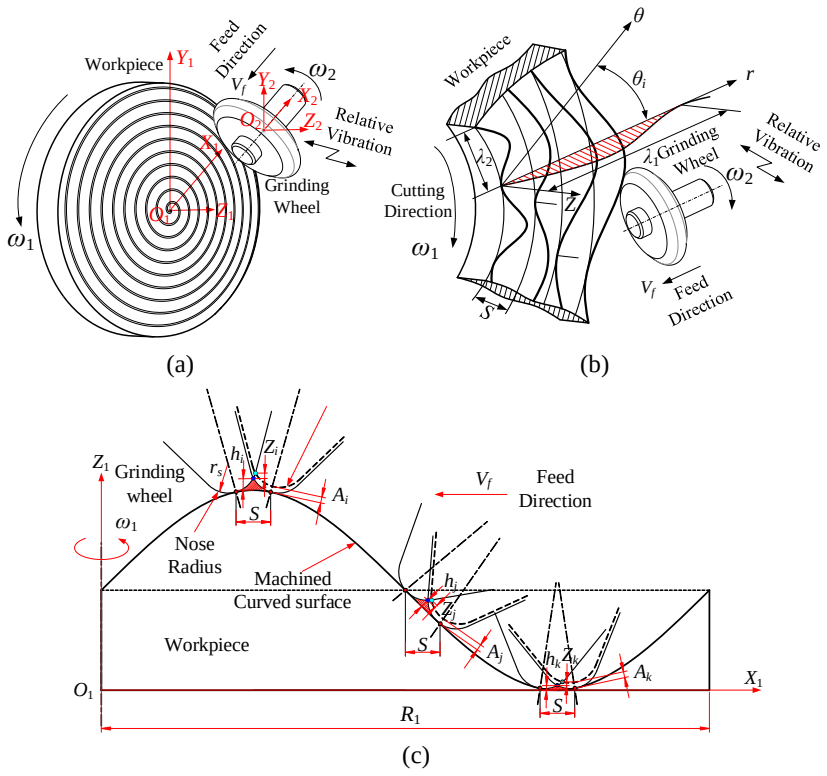

Fig. 1. Schematic of surface waviness formation in the normal grinding of curved surface due to tool vibration (a) tool path, (b) waviness and (c) curvature effect on scallop height.

As shown in Fig. 1(a), the locus of the grinding wheel with respect to workpiece in X-Y plane follows a cycloid path along the spiral tool path, while the workpiece rotates around the center of the workpiece spindle with a transverse feed motion. The linear velocity is different on the workpiece surface in different radial positions. Therefore, the relative linear velocity between the tool and the curved surface is also different. Under interaction between the grinding wheel and workpiece, the lowest point of the grinding wheel leaves the deepest scratch on the ground surface and it has the remarkable impact on the surface generation. Therefore, the formation law of surface microwave can be studied by analyzing the relative kinematic trace of the lowest point with respect to the workpiece surface.

According to the geometric engagement of relative movement between the grinding wheel and workpiece as shown in Fig. 2, the relative locus of the lowest point on the grinding wheel (x_s, y_s,

Optics EXPRESS

z_s) can be calculated as:

$$\begin{cases} x_s = \sin(\omega_1 t) \times [R \times \sin(\omega_2 t) + V_f t - R_1] \quad (0 \le t \le \frac{R_1}{V_f}) \\ y_s = \cos(\omega_1 t) \times [R_1 - R \times \sin(\omega_2 t) + V_f t] \\ z_s = \sqrt{{R_1}^2 - (R_1 - V_f t)^2} + R - R \times \cos(\omega_2 t) + A \sin(\omega_2 t + \varphi) \end{cases} \tag{1}$$

where R is the radius of grinding wheel (mm)

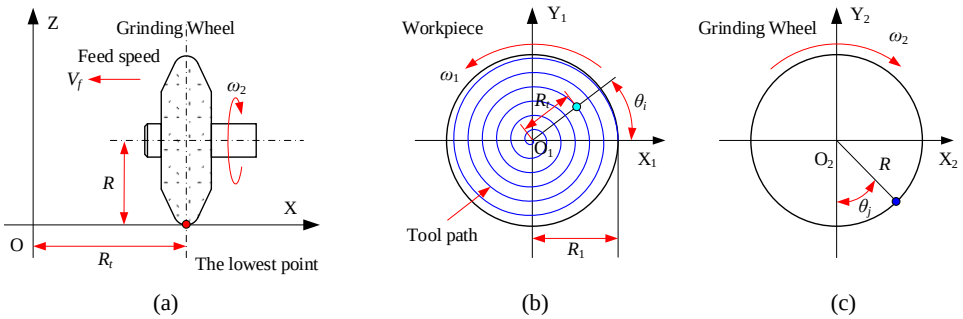

Fig. 2. Schematic of coordinate systems in modelling (a) workpiece-grinding wheel coordinate systems, (b) workpiece coordinate systems and (c) grinding wheel coordinate systems.

V_f is the feed speed (mm/min)
R_1 is the radius of workpiece (mm)
A is the amplitude of vibration (mm)
φ is the initial phase of the wheel vibration (Rad)
t is the machining time (min)
ω_1 is the angular velocity of workpiece spindle (rad/min)
ω_2 is the angular velocity of wheel spindle (rad/min)

3. Influence of curvature effect on scallop height

Previous research suggested that the feed rate is the most primary variable in determining the surface roughness in the parallel grinding [44]. Therefore, the machined surface topography is mainly enveloped by the nose arc of the grinding wheel [44], in which the profile scallop height is mainly determined by the feed rate, wheel geometry and the curvature of workpiece profile in the radical direction. Therefore, the workpiece surface can be divided into a series of cutting planes around the rotation center of workpiece, in which the generated surface profile can be calculated in each cutting plane according to the geometrical relationship between the location of the wheel arc nose and the local curvature of machined surface, as shown in Fig. 3. The surface roughness mainly depends on the height of the residual area along the radial direction in ultra-precision grinding. Therefore, the scallop height is a critical variable to determine the surface roughness and tolerance.

The grinding wheel with a nose radius is adopted for the ultra-precision grinding process, which results in the residual area generation between the two adjacent tool paths. It is assumed that the coordinates of the neighboring two contact points between the tool and workpiece surface are P_i (x_i, y_i, z_i) and P_{i-1} (x_{i-1}, y_{i-1}, z_{i-1}) respectively, and the normal vectors of the curved surface are n_i (n_{ix}, n_{iy}, n_{iz}) and n_{i-1} (n_{i-1x}, n_{i-1y}, n_{i-1z}) respectively, as shown in Fig. 4. In

Optics EXPRESS

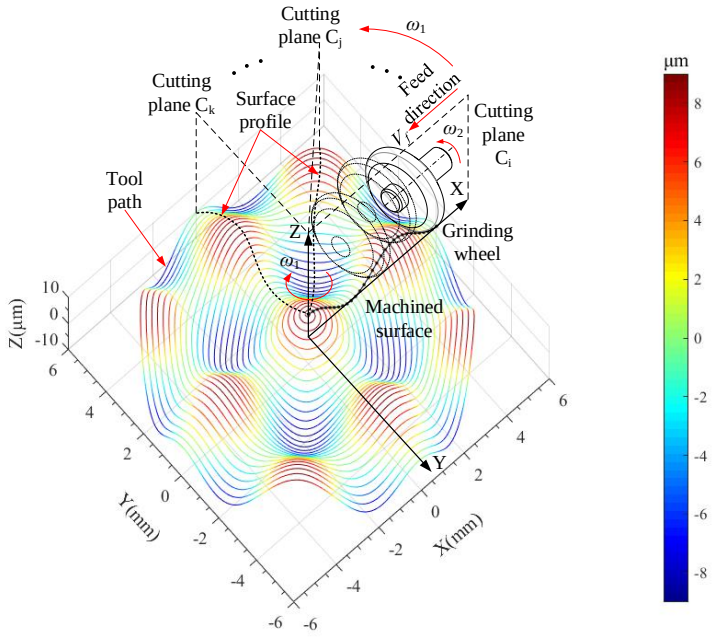

Fig. 3. Geometric representation of cutting plane partition in normal grinding of curved surface.

general, the curvature radius corresponding to P_i and P_{i-1} on the workpiece surface is not equal and the curvature center is not the same.

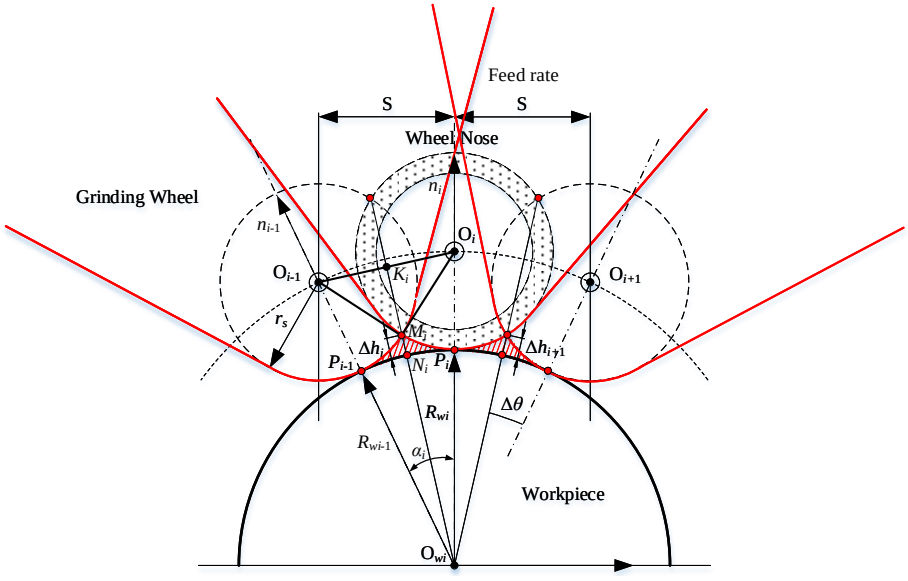

Fig. 4. Geometric representation of scallop height generation in the normal grinding.

Optics EXPRESS

The coordinates of curvature center O_{wi} (x_{wi}, y_{wi}, z_{wi}) are calculated based on the positions and normal vectors of the wheel contact P_i and P_{i-1}, respectively. It can be calculated as follows:

$$\begin{cases} x_{wi} = x_i - R_{wi} \cdot n_{ix} \\ y_{wi} = y_i - R_{wi} \cdot n_{iy} \\ z_{wi} = z_i - R_{wi} \cdot n_{iz} \end{cases} \quad [i = 1, 2 \cdots N = INT(\frac{2R_1}{S})] \tag{2}$$

where R_{wi} is the corresponding curvature radius with respect to cutter contact point.

According to the above analysis, for the neighboring points P_i and P_{i-1} on the curved surface, the difference between the corresponding coordinates of the curvature center ($\Delta x_{wi,\,i-1}$, $\Delta y_{wi,\,i-1}$, $\Delta z_{wi,\,i-1}$) can be derived:

$$(\Delta x_{wi,i-1}, \Delta y_{wi,i-1}, \Delta z_{wi,i-1}) = \begin{bmatrix} x_i - x_{i-1} \\ y_i - y_{i-1} \\ z_i - z_{i-1} \end{bmatrix} - \begin{bmatrix} n_{ix} & -n_{i-1x} \\ n_{iy} & -n_{i-1y} \\ n_{iz} & -n_{i-1z} \end{bmatrix} \cdot \begin{bmatrix} R_{wi} \\ R_{wi-1} \end{bmatrix} \tag{3}$$

Due to the relatively smaller feed span along the X-axis in comparison with the curvature radius of workpiece, it is assumed that two curvature center coordinates of the neighboring P_i and P_{i-1} on the curved surface should be closed. The proximity can be expressed by the sum of squares of the difference between coordinates.

$$J = (\Delta x_{wi,i-1}, \Delta y_{wi,i-1}, \Delta z_{wi,i-1})^T \cdot (\Delta x_{wi,i-1}, \Delta y_{wi,i-1}, \Delta z_{wi,i-1}) \tag{4}$$

$$K = \begin{bmatrix} R_{wi} \\ R_{wi-1} \end{bmatrix} \tag{5}$$

The least squares estimate of K that minimize J, which are obtained by $\frac{\partial J}{\partial K} = 0$.

$$K = \left(\begin{bmatrix} n_{ix} & -n_{i-1x} \\ n_{iy} & -n_{i-1y} \\ n_{iz} & -n_{i-1z} \end{bmatrix}^T \cdot \begin{bmatrix} n_{ix} & -n_{i-1x} \\ n_{iy} & -n_{i-1y} \\ n_{iz} & -n_{i-1z} \end{bmatrix} \right)^{-1} \cdot \begin{bmatrix} n_{ix} & -n_{i-1x} \\ n_{iy} & -n_{i-1y} \\ n_{iz} & -n_{i-1z} \end{bmatrix}^T \cdot \begin{bmatrix} x_i - x_{i-1} \\ y_i - y_{i-1} \\ z_i - z_{i-1} \end{bmatrix} \tag{6}$$

In addition, through the above analysis of geometric relations, it can be concluded that:

$$\begin{cases} R_w = \frac{(R_{wi-1} + R_{wi})}{2} \\ \alpha_i = \cos^{-1}(n_{i-1} \cdot n_i) \end{cases} \tag{7}$$

The value of second partial derivative of curved surface in polar coordinates can be used to determine different types of surface (flat surface, convex and concave surfaces).

$$z'' = f''(r, \theta) = \frac{\partial^2 z}{\partial r^2} \tag{8}$$

For flat surface $z'' = 0$, convex surface $z''<0$, concave surface $z''>0$.

As shown in Fig. 4, in the grinding of convex optical surface, it can be calculated that:

$$\begin{cases} |O_{wi}K_i| = |O_{wi}O_i| \cdot \cos(\frac{\alpha_i}{2}) = (r_s + R_w) \cdot \cos(\frac{\alpha_i}{2}) \\ |M_iK_i| = \sqrt{|O_iM_i|^2 - |O_iK_i|^2} = \sqrt{{r_s}^2 - \left[(R_w + r_s) \cdot \sin(\frac{\alpha_i}{2})\right]^2} \end{cases} \tag{9}$$

where r_s is the nose radius of the grinding wheel (mm)

Optics EXPRESS

The scallop height Δh_i at point N_i in the grinding of the convex surface can be derived as:

$$\begin{aligned}\Delta h_i &= |O_{wi}K_i| - |M_iK_i| - |O_{wi}N_i| \\ &= (r_s + R_w)\cdot\cos(\frac{\alpha_i}{2}) - \sqrt{{r_s}^2 - \left[(R_w + r_s)\cdot\sin(\frac{\alpha_i}{2})\right]^2} - R_w\end{aligned} \tag{10}$$

Similarly, in the grinding of concave surface, the scallop height can be expressed:

$$\Delta h_i = R_w - (r_s - R_w)\cos(\frac{\alpha_i}{2}) - \sqrt{{R_w}^2 - [(R_w - r_s)\sin(\frac{\alpha_i}{2})]^2} \tag{11}$$

In normal grinding, the unbalanced vibration of the grinding wheel leads to the further increase for scallop height. According to the geometric relation of the relative movement of the grinding wheel, as shown in Fig. 5, the increase of scallop height ΔZ_i can be calculated as:

$$\begin{cases} \Delta Z_i = \frac{S\sqrt{4r_s - \Delta A_{zi}{}^2} - \Delta A_{zi}\sqrt{(r_s+R_w)^2 - S^2}}{r_s + R_w} - \sqrt{r_s - \frac{S^2}{4}} \\ R_w = \frac{(R_{wi-1}+R_{wi})}{2} \\ \Delta A_{zi} = A\sin(\omega_2 t_i + \varphi) - A\sin[\omega_2(t_i + \frac{2\pi}{\omega_2}) + \varphi] \end{cases} \tag{12}$$

where ΔA_i is the height difference between i th and $i-1$th tool path (mm)

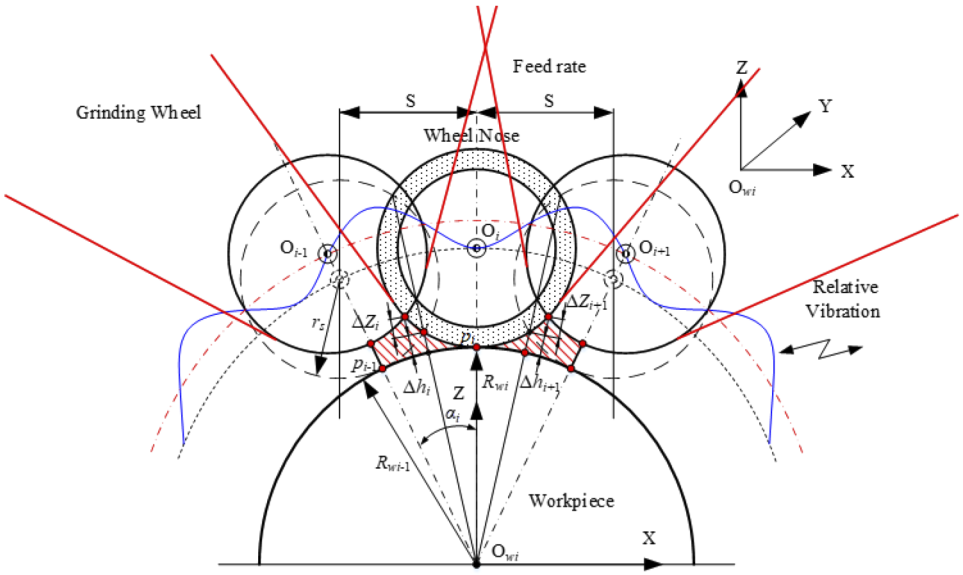

Fig. 5. Scallop height increased caused by the relative vibration of grinding wheel.

x_i is the distance that wheel moved towards to the center of workpiece (mm)

φ is the unbalanced vibration phase of the grinding wheel (Rad)

From the above theoretical modelling of the scallop height, it can be found that the surface scallop height is mainly determined by the tool feed rate and the curvature of workpiece surface profile. Therefore, for the specified allowable value of scallop height ΔH_i=Δh_i+ΔZ_i, the feed rate can be adjusted according to the local curvature of workpiece surface profile. For a given scallop height, the feed rate of the grinding wheel S with respect to different curvatures can be

Optics EXPRESS

calculated according to Eq. (10)–Eq. (12), therefore the feed speed V_f can be derived as:

$$\begin{cases} V_f = n_1 S = n_1 \frac{(R_w+r_s)[(\Delta H_i-\Delta h_i+r_s)\sqrt{4{r_s}^2-\Delta {A_{zi}}^2}-\sqrt{(4{r_s}^2-\Delta {H_i}^2)(\Delta H_i-\Delta h_i+r_s)^2+4{r_s}^2\Delta {A_{zi}}^2}]}{4{r_s}^2} \\ \Delta A_{zi} = A\sin(\omega_2 t_i+\varphi) - A\sin[\omega_2(t_i+\frac{2\pi}{\omega_2})+\varphi] \\ R_w = \frac{(R_{wi-1}+R_{wi})}{2} \\ \Delta H_i = \Delta h_i + \Delta Z_i \end{cases} \tag{13}$$

where n_1 is the workpiece spindle speed (RPM)

ΔH_i is the specified allowable value of scallop height (mm)

For a given allowable value of scallop height ΔH_i, The feed speed V_f can be determined by Eq. (13) and the surface scallop height can be controlled.

4. Experimental results and discussion

4.1. Experimental setup

It is found that the scallop height (ΔH_i) has a direct relationship with feed speed (V_f) and the local curvature of the machined surface ($1/R_w$) from the previous theoretical analysis. If the grinding operation parameters and the wheel tool geometry are given, then the scallop height is mainly determined by the machined surface curvature. It is known that surface scallop height is an important factor to determine the surface roughness and surface topography, which directly determines the performance of the grinding operation.

The grinding experiment is conducted on an ultra-precision grinder with 4-axis (Moore Nanotech 450 UPL). The workpiece spindle (C-axis) is perpendicular to the X-axis guide slide (T-shaped layout) and workpiece is fixed by a vacuum chuck. The C-axis is installed on the X guide slide and the grinding wheel spindle is fixed on the Z-axis guide slide with a rotating B-axis, which can swing at a setting angle, as shown in Fig. 6. The grinder has the capacity of machining various types of curved surface, such as toric, aspheric, micro-lens array and freeform

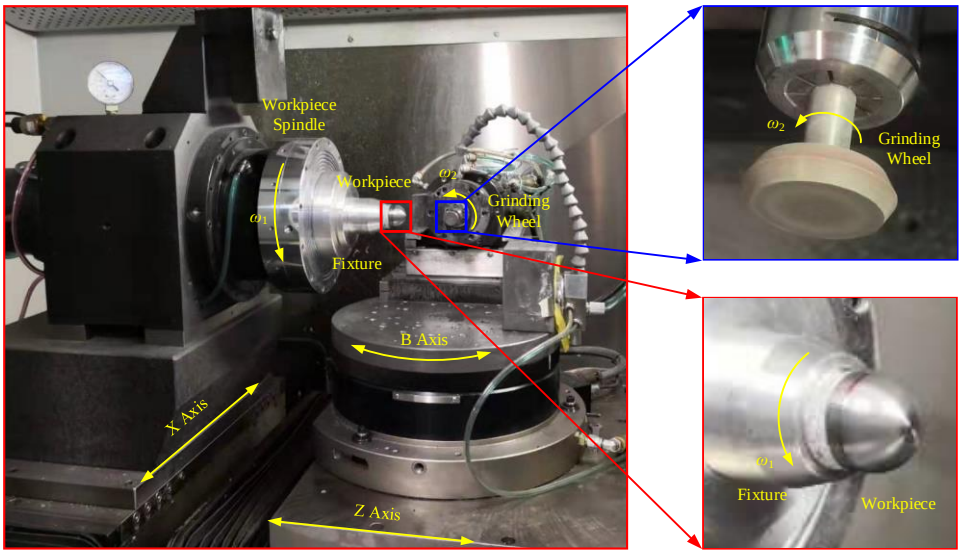

Fig. 6. Experimental setup of the normal grinding of curved surface.

Optics EXPRESS

surface. Figure 7 shows the schematic of relative movement between the wheel and workpiece in the normal grinding operation.

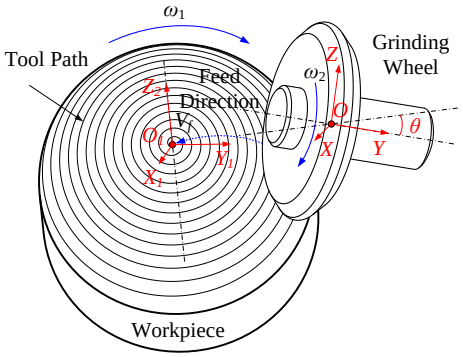

Fig. 7. Schematic of relative motion between the workpiece and wheel in the normal grinding.

Resin bonded diamond wheel (#1500-grit) is adopted in the experiment, its conditions include: wheel radius=10 mm, thickness=5 mm, nose radius=0.5 mm and tungsten carbide (WC) is selected as machined material. Due to the fact that the main motion error of the grinding wheel is related to its rotational speed, therefore, the wheel speed is kept n_2=40000 RPM through all experiments.

Since the surface condition of grinding wheel has a significant effect on the surface generation and surface quality, the dressing and sharpening process are very important. In order to reduce the effect of the change in the wheel surface conditions, the same parameters are used for dressing and truing the grinding wheels before each experiment. In addition, the wheel wear poses adverse effect on surface quality and shape accuracy, which resulted in the changes of contact area between the workpiece and the wheel in grinding of curved surface. In order to reduce the influence of the grinding wheel wear on ground surface topography, rough and fine grinding operation are conducted to get desired surface shape and quality before the experiments.

In order to calculate the relative influence of the curvature on the ground surface quality, the Taguchi experiment method is adopted and the impact of the workpiece speed, depth of cut, feed speed and workpiece curvature on the surface roughness is studied. In the Taguchi experiment design, a combination of four factors (each factor has three levels) is selected and an orthogonal array L9 (3^4) is arranged to study their corresponding impacts on surface generation. Grinding operation parameters were selected at three different levels, which include workpiece spindle speed (n_1) in the range of 500 RPM to 1500 RPM, depth of cut (a_p) increased from 5 μm to 15 μm, and feed speed (V_f) changed from 5 mm/min to 15 mm/min, the curvature radius varied from 5 mm to 15 mm, as shown in Table 1. Finally, the surface roughness for each experiment is obtained and the signal-to-noise ratio (S/N) for the smaller is better characteristic is calculated, which is used to evaluate the surface roughness characteristics and determine the relative impact of the four factors.

4.2. Results and discussion

Table 2 and Table 3 show the main effect and average factor S/N responses for arithmetic mean area surface roughness Sa, respectively. It can be observed that the relative influence order of grinding variables on surface roughness is: rotational speed of workpiece spindle > feed speed > surface curvature > depth of cut, as shown in Table 4. The influence of workpiece speed, feed speed and depth of cut on surface quality was analyzed in our previous publication. It is found

Optics EXPRESS

Table 1. Experimental design variables and levers

No.	Technical parameters	Levels		
		1	2	3
A	n_1 (RPM)	500	1000	1500
B	a_p (μm)	5	10	15
C	V_f (mm/min)	5	10	15
D	$1/R_w$ (mm^{-1})	1/15	1/10	1/5

that the curvature tolerance $\Delta = 0.1723$ is quite close to that of the feed speed, which shows the influence of curvature on the surface roughness is significant, as shown in Fig. 8. It indicates that the influence of curvature on the surface quality cannot be ignored.

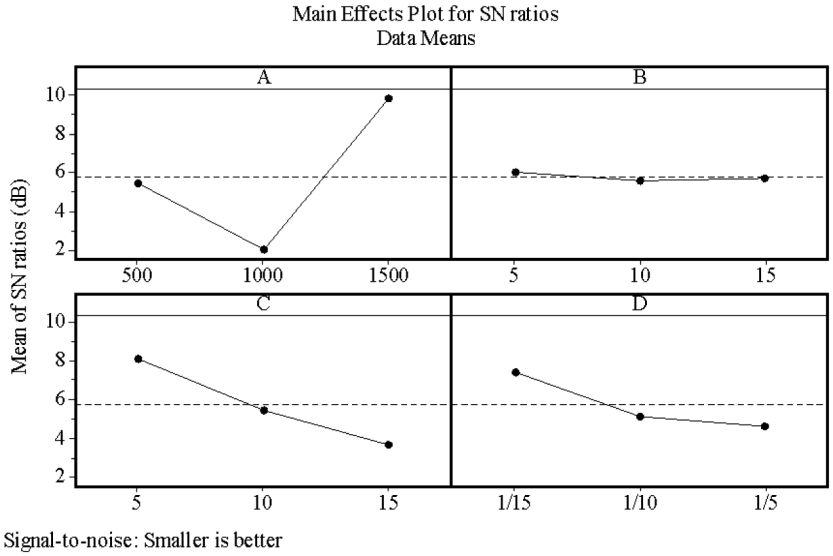

Fig. 8. Main effect of S/N ratio graph for Sa.

Table 2. Experimental results for Sa

No.	Technical parameters				
	A	B	C	D	Sa (μm)
1	500	5	5	1/15	0.327
2	500	10	10	1/10	0.606
3	500	15	15	1/5	0.779
4	1000	5	10	1/5	0.901
5	1000	10	15	1/15	0.843
6	1000	15	5	1/10	0.656
7	1500	5	15	1/10	0.424
8	1500	10	5	1/5	0.283
9	1500	15	10	1/15	0.276

The Nexview 3D optical profiler microscope is adopted to measure the topography of ground surface after machining, in which the tilt error and the spherical form of measured surface are

Optics EXPRESS

Table 3. S/N ratio response of main factor for Sa

Technical parameters	Levels			Δ	Rank
	1	2	3		
A	5.410	2.017	9.866	7.849	1
B	6.022	5.599	5.671	0.423	4
C	8.112	5.479	3.702	4.410	2
D	7.458	5.155	4.680	2.778	3

Table 4. S/N ratio response of mean factor for Sa

Technical parameters	Levels			Δ	Rank
	1	2	3		
A	0.5707	0.8000	0.3277	0.4723	1
B	0.5507	0.5773	0.5703	0.0267	4
C	0.4220	0.5943	0.6820	0.2600	2
D	0.4820	0.5620	0.6543	0.1723	3

removed. It is observed that micro-waviness remarkably existed on the ground surface, which results from the unbalanced vibration of the wheel, as shown in Fig. 9. The protruding areas are the vibration marks, the spatial scale is larger than feed marks on the ground surface. The unbalanced vibration of the wheel is difficult to eliminate in high-speed grinding even if both of fine static and dynamic balance work have been carried out before machining operation, in which slight wear nonuniformity for the wheel is liable to cause unbalanced tool vibration. In our previous study, the number of micro-waviness around the rotational center of workpiece is equal to the speed ratio between the wheel and workpiece, which indicates that the period of vibration is equivalent to the time for grinding wheel complete one revolution, therefore, it is essential to know the actual rotational speed of the wheel in the operation [31]. By recording 10 actual values of rotational speed for the wheel and get the average speed, it is found that the actual speed of the wheel is approximately 22 RPM larger than the presetting speed. Ultra-high-speed laser displacement sensor (KEYENCE LK-H022) is adopted and sampling interval is set at 0.01 μs to measure the amplitude and frequency of wheel vibration, as shown in Fig. 10. The main vibration amplitude and frequency are equal to approximately 2.5 μm and 667 Hz, in which the vibration frequency is equal to the wheel rotation frequency as shown in Fig. 11.

To investigate the mechanism of micro-waviness formation in the grinding of spherical surface, the simulation of vibration marks is carried out and it is found that the vibration marks agree well with the experiments, as shown in Fig. 12.

From Eqs. (9–11), it is found that the curvature of the workpiece surface has an important impact on the scallop height of the ground surface. In order to further investigate the influence of the curvature on the surface scallop height, the workpiece with different spherical radii (R_w=5 mm, R_w=10 mm and R_w=15 mm) are selected. It is observed that under the same processing conditions (workpiece spindle speed n_1=1500 RPM, wheel spindle speed n_2=40000 RPM, feed speed V_f = 5 mm/min, depth of cut a_p=5 μm), the geometry of vibration mark is almost the same for different curvatures under same machining parameters, but the surface scallop height and roughness profile vary with the change of surface profile curvature, larger curvature (smaller curvature radius) results in larger amplitude of scallop height, as shown in Fig. 13. The results are consistent with the Taguchi analysis, it shows that the change of curvature can lead to the variation of profile height of machined surface and contributed to the uneven distributed scallop height in the grinding of curved surface with various curvature radii.

Optics EXPRESS

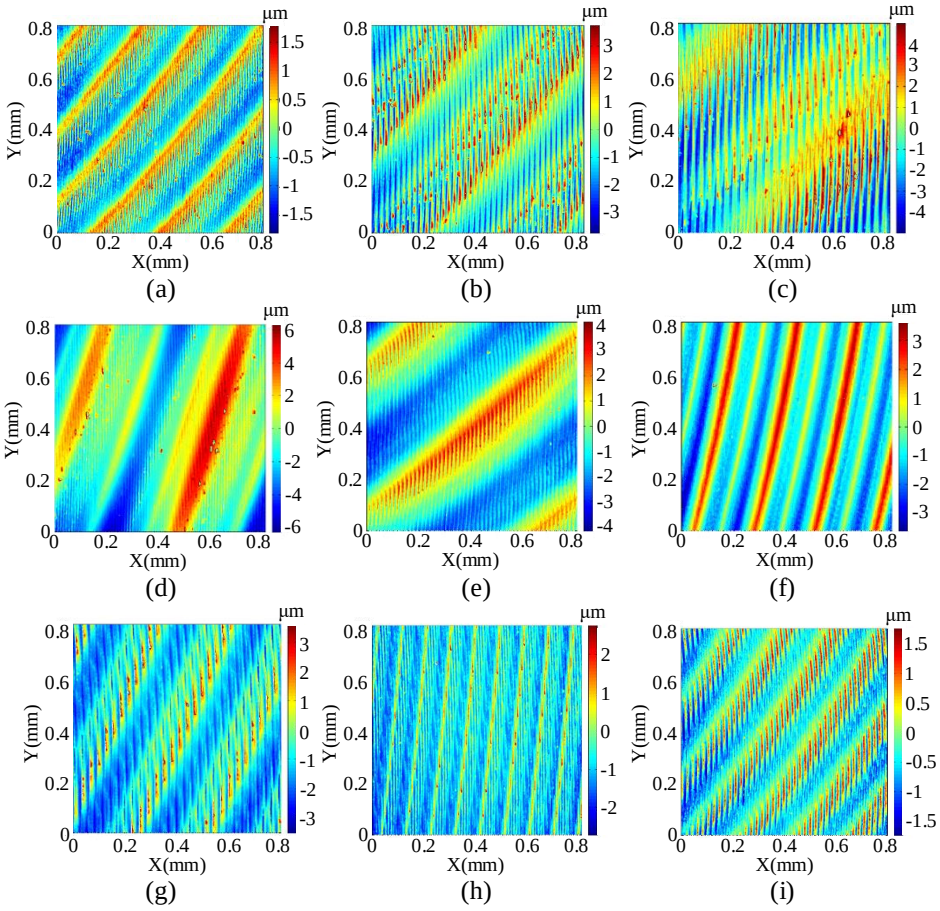

Fig. 9. Measured surface topography in grinding of spherical surface (remove the form).

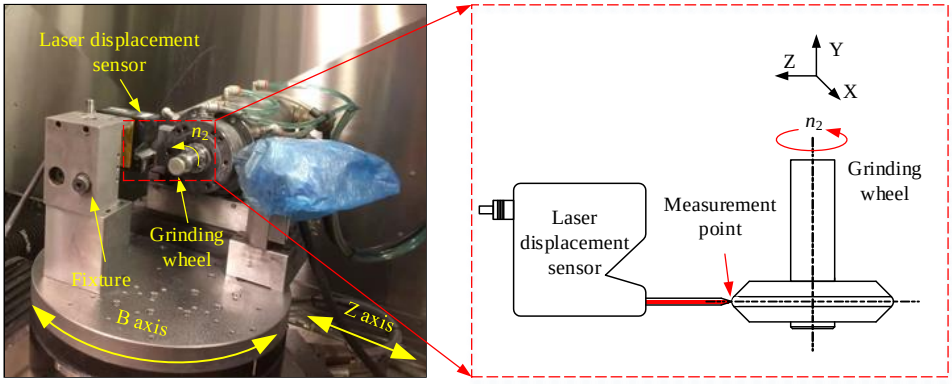

Fig. 10. Schematic of measuring the amplitude and frequency of wheel vibration by using a laser displacement sensor in the grinding

Optics EXPRESS

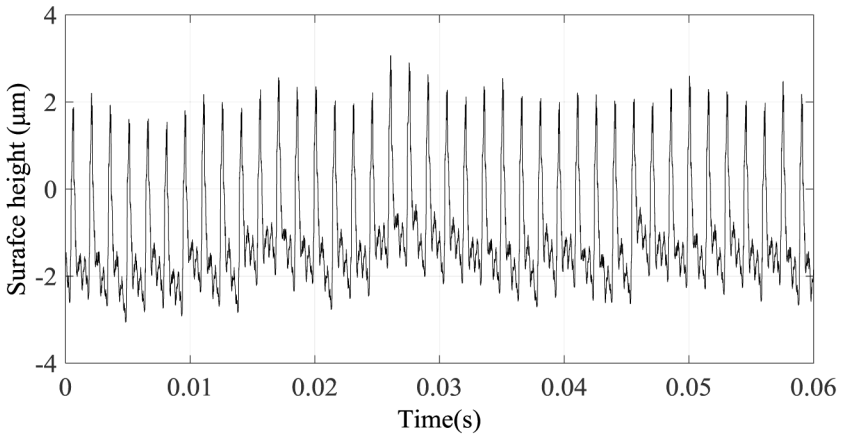

Fig. 11. The measurement results of grinding wheel relative displacement by using a laser displacement sensor (rotational speed of the grinding wheel = 4000RPM)

It indicates that curvature is an important variable to surface generation and surface quality. In order to improve the surface quality of the workpiece and control the surface scallop under varying curvatures based on the previous theoretical model of scallop height, the cutter location data (feed speed) on the workpiece surface can be calculated based on the relationship between the curvature and the scallop height, which can be used to control the scallop height for achieving the uniform surface quality.

In order to verify the model and achieve the control of surface scallop height in the normal grinding, in the experiment, taking the micro sinusoidal array surface as an example, it can be expressed in Eq. (14). Figure 14 and Fig. 15 show the designed the micro sinusoidal array surface and its curvature distribution map respectively.

$$z = f(\rho, \theta) = A_x \sin(\frac{2\pi\rho\cos\theta}{\lambda_x}) + A_y \sin(\frac{2\pi\rho\sin\theta}{\lambda_y}) \tag{14}$$

where A_x is the amplitude of sine wave in X direction, mm;

A_y is the amplitude of sine wave in Y direction, mm;

λ_x is the wavelength of sine wave in the X direction, mm;

λ_y is the wavelength of sine wave in the Y direction, mm;

Figure 16 and Fig. 17 show the micro sinusoidal array surface machined by adopting conventional method (constant feed speed $V_f = 5$ mm/min) and scallop height control algorithm respectively (grinding operation condition: n_1=1500 RPM, $n_2 = 40000$ RPM, a_p=5 μm). It can be observed that the micro sinusoidal array is evenly distributed and has the same size with the designed micro sinusoidal array as shown in Fig. 17. In order to detect the ground surface profile of sinusoidal array in different areas with respect to different curvatures, the measured area is divided into peak, trough and relative flat area, as shown in Fig. 16 and Fig. 17. Figure 18 represents the contour diagram of the machined micro sinusoidal array. It is observed that the wavelength and amplitude of micro sinusoidal array is consistent with the designed value. Figure 19 and Fig. 20 compares surface scallop height profile with respect to different curvatures between conventional grinding and scallop height control grinding method. It is found that the amplitude of scallop height is very nonuniform with the changes of curvature over the surface, in which the scallop height is obviously larger in peak and trough of sine wave than that of flat position of sine wave, as shown in Fig. 19(a), Fig. 19(b) and Fig. 19(c). However, adopting proposed feed speed control method, the surface profile height at the peak and trough area where sinusoidal wave curvature changes sharply are consistent with that of the relative flat region and

Optics EXPRESS

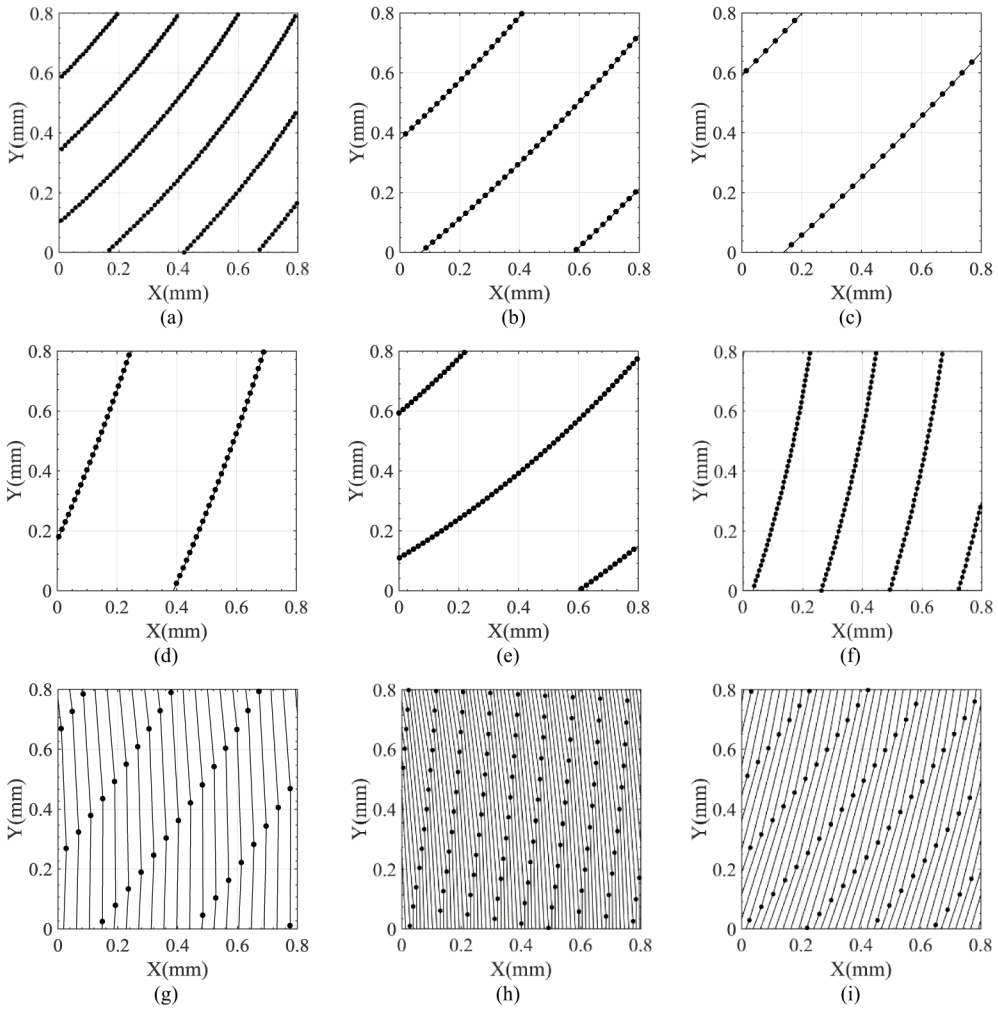

Fig. 12. Simulated 2D micro-waviness marks for grinding of spherical surface (X-Y plane) in Taguchi experiment respectively.

Optics EXPRESS

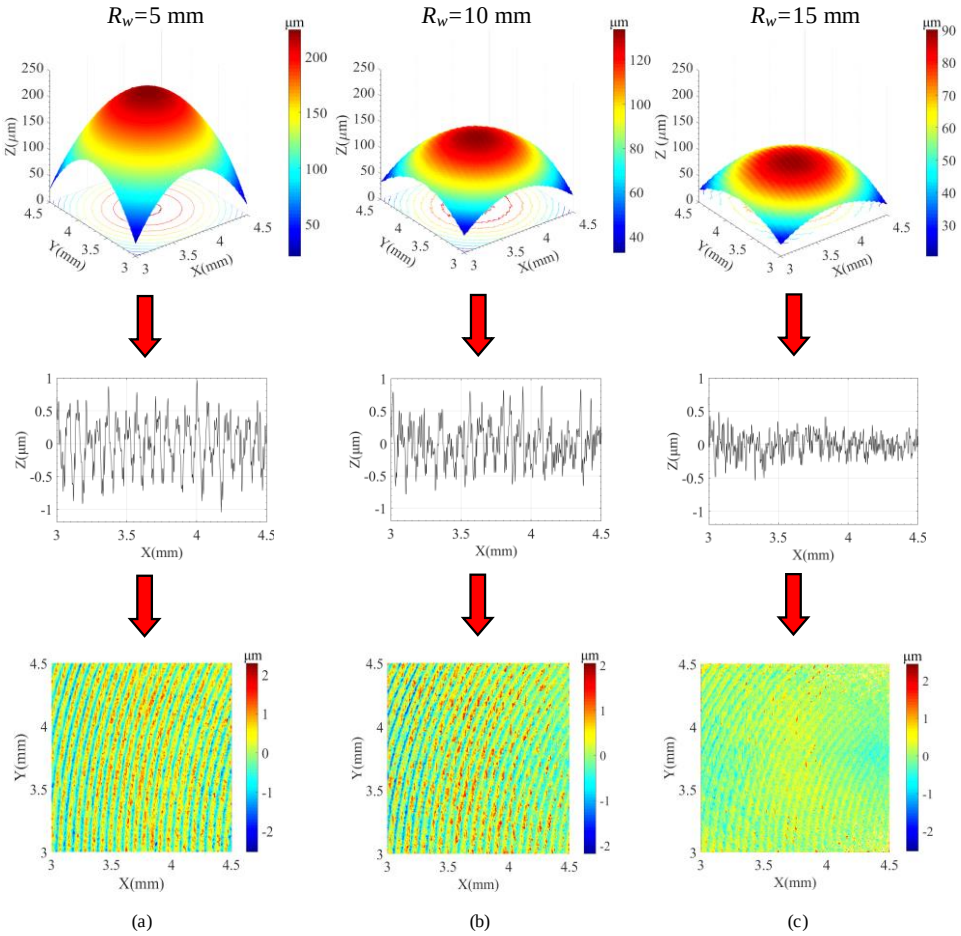

Fig. 13. The influence of curvature on scallop height (45 degree tilt in measurement).

the amplitude of ground surface profile is basically located between −0.03 μm and 0.03 μm (the setting value for scallop height ΔH=0.06 μm), while the surface roughness is also hold constant at 0.02 μm approximately, as shown in Fig. 20(a), Fig. 20(b) and Fig. 20(c). It indicates that the machining of uniform and super smooth surfaces can be achieved by using the tool control algorithm of scallop height in the normal grinding of curved surface.

To further verify the model of uniform scallop height generation in grinding of curved surface, surface matching is conducted. The measured and simulated surface data are transformed into the same coordinate system to calculate the error map as shown in Fig. 21, which can be used to determine the machining errors [45]. The iterative closest points (ICP) algorithm is frequently used to surface matching, in which the optimal transformation parameters both for translation and rotation matrices are determined for two-point sets to minimize surface registration errors. Figure 22 and Fig. 23 show the matching results for machined surfaces ground by conventional method and proposed scallop height control method respectively, it is observed that the surface uniformity and shape accuracy are improved remarkably by adopting scallop height control algorithm.

Optics EXPRESS

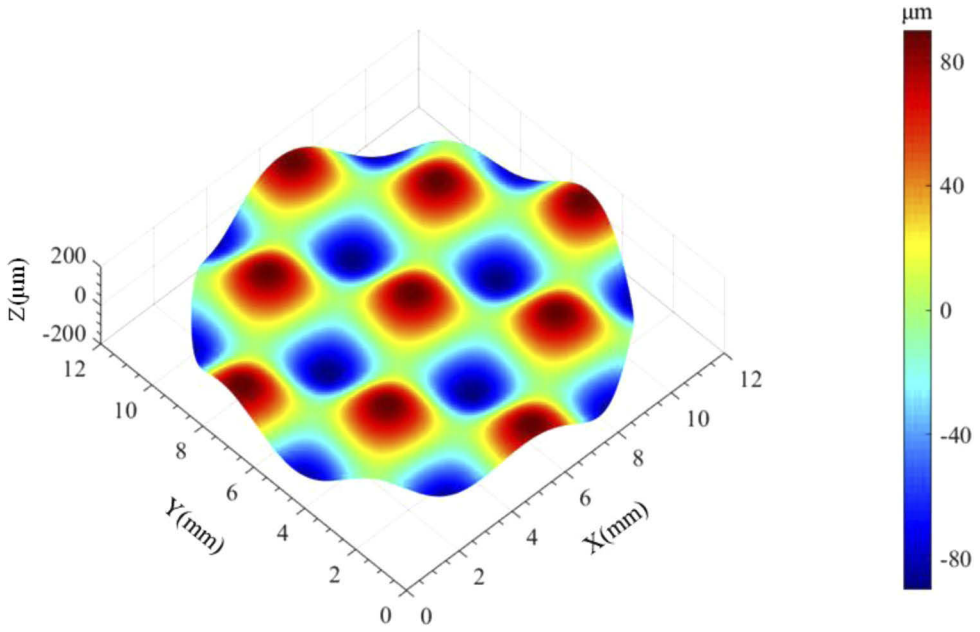

Fig. 14. Designed the micro sinusoidal array ($A_x = A_y = 0.045$ *mm*; $\lambda_x = \lambda_y = 4$ *mm*).

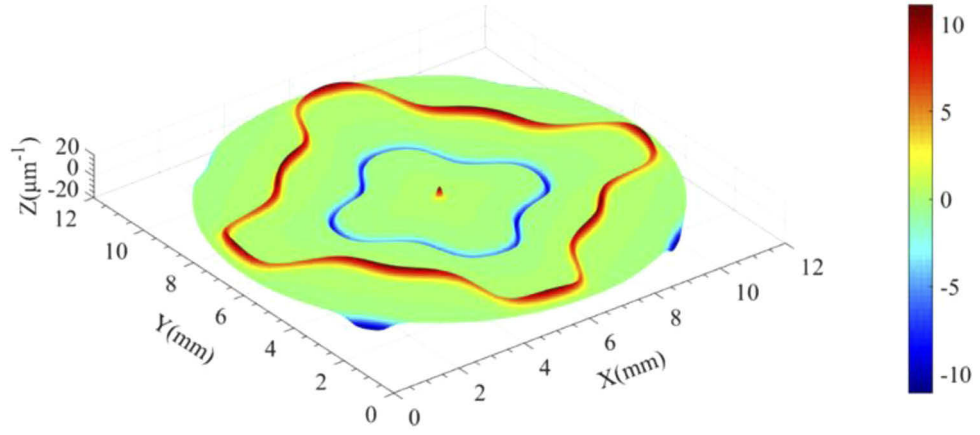

Fig. 15. The curvature distribution for micro sinusoidal array ($A_x = A_y = 0.045$ *mm*; $\lambda_x = \lambda_y = 4$ *mm*).

Optics EXPRESS

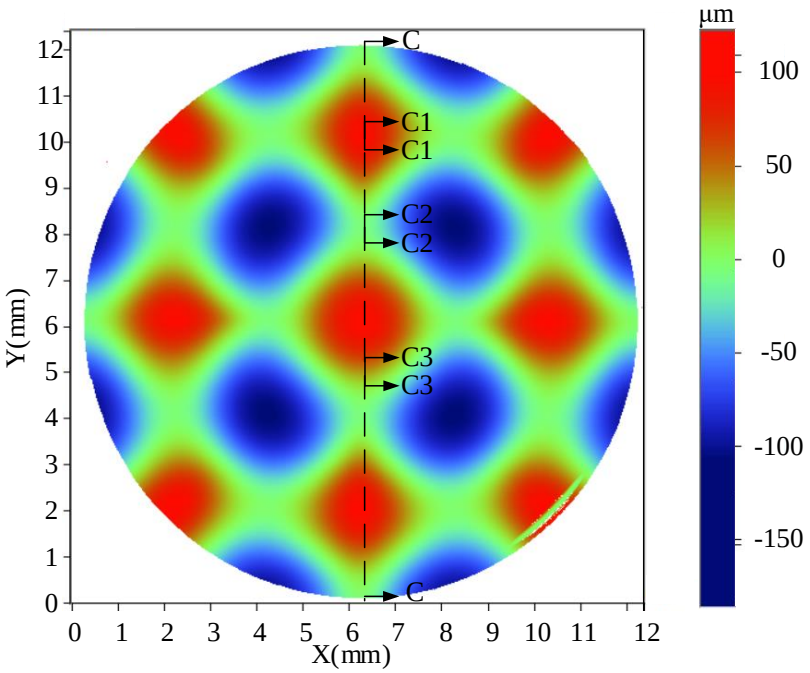

Fig. 16. Illustration of measured area division and measured topography (constant feed speed).

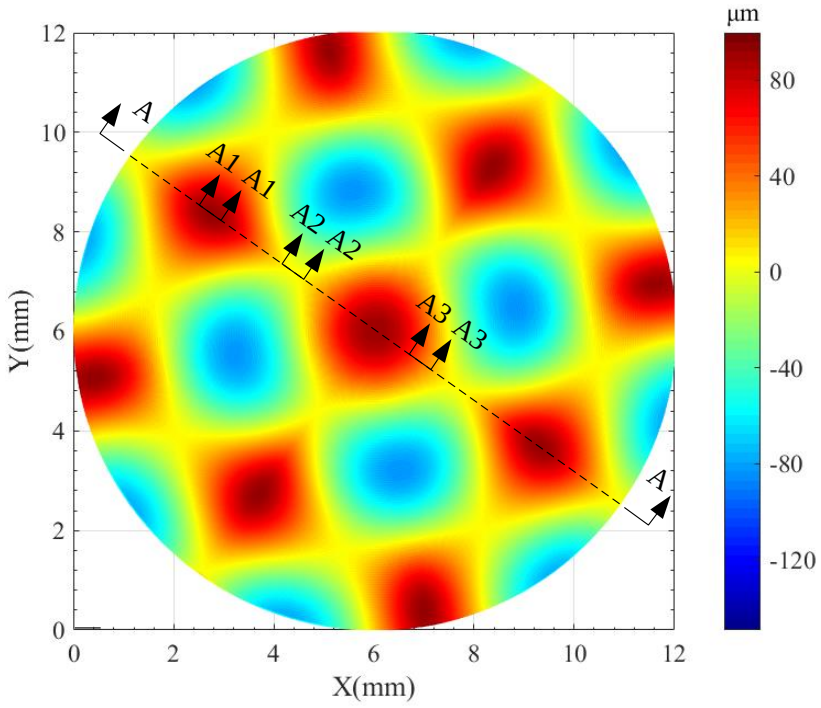

Fig. 17. Illustration of measured area division and measured topography (variable feed speed).

Optics EXPRESS

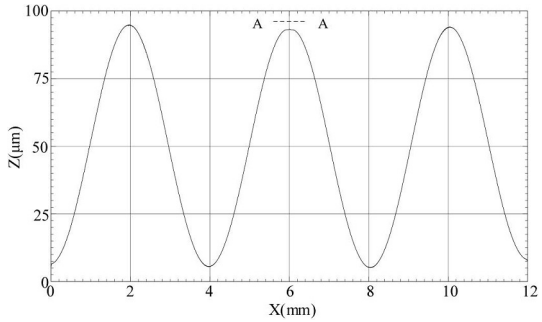

Fig. 18. Surface profile of machined micro sinusoidal array.

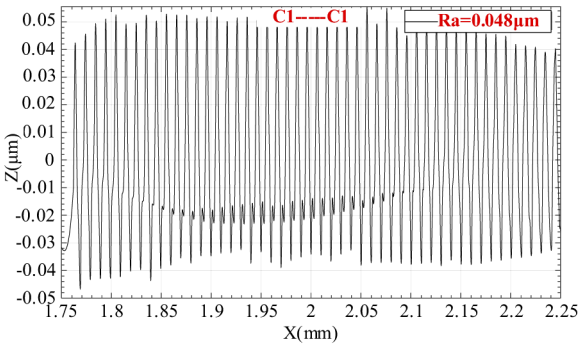

(a) The profile of peak of sine wave

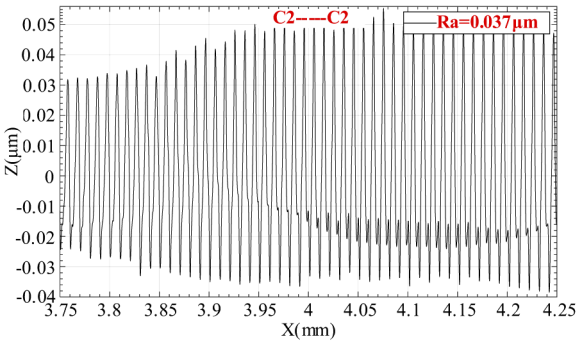

(b) The profile of trough of sine wave

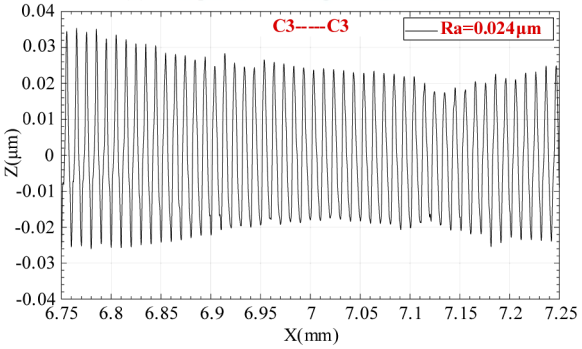

(c) The profile of flat position of sine wave

Fig. 19. Surface profiles of micro sinusoidal array: conventional method (constant feed speed)

Optics EXPRESS

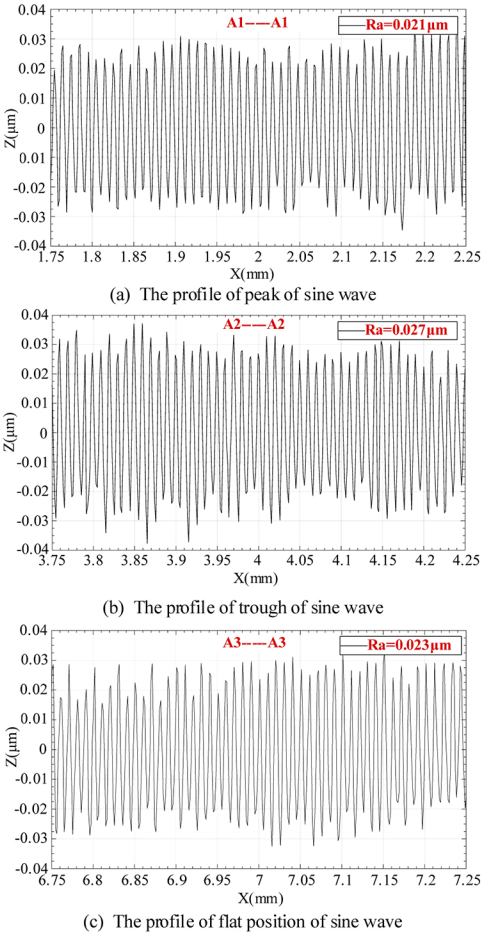

(a) The profile of peak of sine wave

(b) The profile of trough of sine wave

(c) The profile of flat position of sine wave

Fig. 20. Surface profiles of micro sinusoidal array with respect to different curvatures: proposed scallop height control method (variable feed speed).

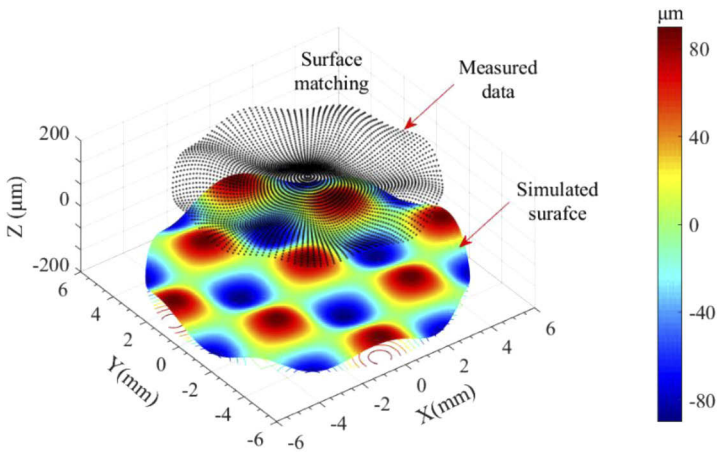

Fig. 21. Sketch of surface matching for error evaluation

Optics EXPRESS

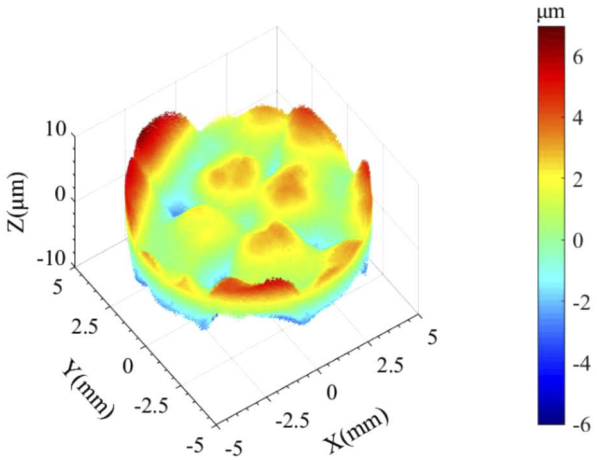

Fig. 22. Error map for conventional grinding method (Constant feed speed)

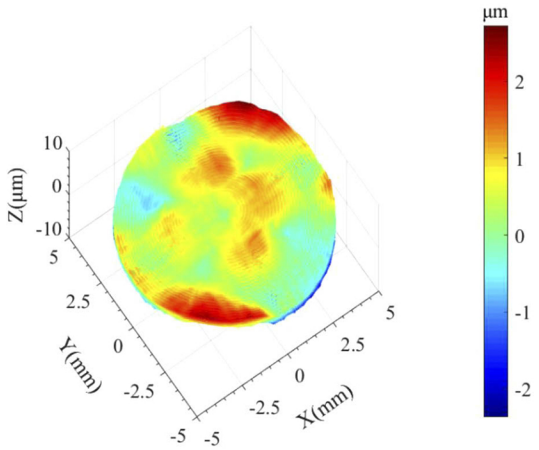

Fig. 23. Error map for proposed scallop height control method (variable feed speed)

5. Conclusions

Normal grinding technology has been frequently used to fabricate many types of complex curved surface, the change of curvature on the machined surface posed adverse effect on surface quality and profile accuracy. In this paper, an experimental and theoretical investigation of influence of curvature on the surface topography generation is conducted to enhance the controllability of surface uniformity in the grinding of curved surface. For the grinding of complex curved surface, the frequent change of curvature poses a challenge work for obtaining uniform surface topography and high shape accuracy. The proposed scallop height control method is capable of obtaining high homogeneity and desired surface quality in the grinding of complex surface. The main conclusions are the following several aspects:

(1) In the normal grinding of curved surface, the micro-waviness is the principal feature of surface generation resulted from the grinding wheel vibration and the surface curvature makes no significant in waviness geometry evolution (in X-Y plane).

Optics EXPRESS

(2) Surface curvature has a great impact on the scallop height, which leads to different scallop height between neighbouring grinding paths, the smaller the curvature, the smaller the scallop height.

(3) A novel scallop height model is established by considering relative vibration of the machine tool, cutting tool geometry and surface curvature, in which the scallop height can be controlled by feed speed according to the local curvature of workpiece surface profile.

(4) The micro sinusoidal array is ground through controlling the magnitude of feed speed corresponding to the surface curvature change. Results show that the surface scallop height is consistent with the setting value regardless of the machined area with large curvature or gentle curvature and the surface roughness is kept uniform over the machined surface. It shows that the model can be exploited to feasibly control the homogeneous and super-smooth surface generation in normal grinding of optical components.

Funding. China Postdoctoral Science Foundation (2019M663681); Program for Science and Technology Innovation Group of Shaanxi Province (2019TD-011); Key Research and Development Projects of Shaanxi Province (2020ZDLGY04-02); National Science Fund for Excellent Young Scholars (51722509); National Key Research and Development Program of China (2017YFB1104700); Scientific Research and development plan for Beilin District (Xi'an city, Shaanxi Province) 2020 (GX2028); Natural Science Foundation of Zhejiang Province (LQ21E050010); China Scholarships Council (202006285057); Department of Industrial and Systems Engineering, The Hong Kong Polytechnic University (RU3K).

Disclosures. The authors declare no conflicts of interest.

References

1. K. S. Alexander, T. Jonas, and V. Urs, "Ocular wavefront analysis of aspheric compared with spherical monofocal intraocular lenses in cataract surgery: systematic review with metaanalysis," J. Cataract Refractive Surg. **41**(5), 1088–1097 (2015).
2. S. J. Zhang, Y. P. Zhou, H. J. Zhang, Z. W. Xiong, and S. To, "Advances in ultra-precision machining of micro-structured functional surfaces and their typical applications," Int J Mach Tool Manu **142**, 16–41 (2019).
3. G. J. Ding, R. J. He, K. Q. Zhang, N. P. Zhou, and H. Xu, "Stereolithography 3D printing of SiC ceramic with potential for lightweight optical mirror," Ceram. Int. **46**(11), 18785–18790 (2020).
4. E. Brinksmeier, Y. Mutlugünes, F. Klocke, J. C. Aurich, P. Shore, and H. Ohmori, "Ultra-precision grinding," CIRP Ann. **59**(2), 652–671 (2010).
5. V. Mishra, D. R. Burada, K. K. Pant, V. Karar, S. Jha, and G. S. Khan, "Form error compensation in the slow tool servo machining of freeform optics," Int J Adv Manuf Technol **105**(1-4), 1623–1635 (2019).
6. P. He, L. K. Li, H. Li, J. F. Yu, L. J. Lee, and A. Y. Yi, "Compression molding of glass freeform optics using diamond machined silicon mold," Manuf. Lett. **2**(2), 17–20 (2014).
7. F. Z. Fang, X. D. Zhang, A. Weckenmann, G. X. Zhang, and C. Evans, "Manufacturing and measurement of freeform optics," CIRP Ann. **62**(2), 823–846 (2013).
8. W. Choi, J. Y. Lee, W. B. Kim, B. K. Min, S. Kang, and S. J. Lee, "Design and fabrication of tungsten carbide mould with micro patterns imprinted by micro lithography," J. Micromech. Microeng. **14**(11), 1519–1525 (2004).
9. B. Guo, Q. L. Zhao, and M. J. Jackson, "Precision grinding of binderless ultrafine tungsten carbide (WC) microstructured surfaces," Int J Adv Manuf Technol **64**(5-8), 727–735 (2013).
10. H. Suzuki, M. Okada, Y. Yamagata, S. Morita, and T. Higuchi, "Precision grinding of structured ceramic molds by diamond wheel trued with alloy metal," CIRP Annals **61**(1), 283–286 (2012).
11. M. T. Wu, B. Guo, Q. L. Zhao, and P. He, "Precision grinding of a microstructured surface on hard and brittle materials by a microstructured coarse-grained diamond grinding wheel," Ceram. Int. **44**(7), 8026–8034 (2018).
12. C. L. He, W. J. Zong, and T. Sun, "Origins for the size effect of surface roughness in diamond turning," Int J Mach Tool Manu **106**, 22–42 (2016).
13. Y. Yang, H. N. Li, Z. R. Liao, D. Axinte, W. L. Zhu, and A. Beaucamp, "Controlling of compliant grinding for low-rigidity components," Int J Mach Tool Manu **152**, 103543 (2020).
14. O. G. Diaz, G. G. Luna, Z. R. Liao, and D. Axinte, "The new challenges of machining Ceramic Matrix Composites (CMCs): Review of surface integrity," Int J Mach Tool Manu **139**, 24–36 (2019).
15. Z. R. Liao, A. Abdelhafeez, H. N. Li, Y. Yang, O. G. Diaz, and D. Axinte, "State-of-the-art of surface integrity in machining of metal matrix composites," Int J Mach Tool Manu **143**, 63–91 (2019).
16. C. L. He, W. J. Zong, and J. J. Zhang, "Influencing factors and theoretical modeling methods of surface roughness in turning process: State-of-the-art," Int J Mach Tool Manu **129**, 15–26 (2018).
17. C. L. He and W. J. Zong, "Influencing factors and theoretical models for the surface topography in diamond turning process: A review," Micromachines **10**(5), 288 (2019).
18. Q. Liu, Z. R. Liao, and D. Axinte, "Temperature effect on the material removal mechanism of soft-brittle crystals at nano/micron scale," Int J Mach Tool Manu **159**, 103620 (2020).

Optics EXPRESS

19. Y. C. Pan, Q. L. Zhao, B. Guo, B. Chen, and J. H. Wang, "Suppression of surface waviness error of fresnel micro-structured mold by using non-integer rotation speed ratio in parallel grinding process," Micromachines **11**(7), 652 (2020).
20. C. Li, X. L. Li, S. Q. Huang, L. Q. Li, and F. H. Zhang, "Ultra-precision grinding of $Gd_3Ga_5O_{12}$ crystals with graphene oxide coolant: Material deformation mechanism and performance evaluation," J. Manuf. Process **61**, 417–427 (2021).
21. H. C. Chuang and P. L. Tso, "An investigation of lapping characteristics for improving the form error of an aspheric lens," J. Mater. Process. Technol. **176**(1-3), 183–190 (2006).
22. X. Zhou and F. Xi, "Modeling and predicting surface roughness of the grinding process," Int J Mach Tool Manu **42**(8), 969–977 (2002).
23. C. Li, X. L. Li, Y. Q. Wu, F. H. Zhang, and H. Huang, "Deformation mechanism and force modelling of the grinding of YAG single crystals," Int J Mach Tool Manu **143**, 23–37 (2019).
24. J. Wu, J. Cheng, C. Gao, T. Yu, and Z. Z. Guo, "Research on predicting model of surface roughness in small-scale grinding of brittle materials considering grinding tool topography," Int. J. Mech. Sci. **166**, 105263 (2020).
25. C. Li, Y. Q. Wu, X. L. Li, L. J. Ma, F. H. Zhang, and H. Huang, "Deformation characteristics and surface generation modelling of crack-free grinding of GGG single crystals," J. Mater. Process. Technol. **279**, 116577 (2020).
26. H. P. Xiao, Z. Chen, H. R. Wang, J. H. Wang, and N. Zhu, "Effect of grinding parameters on surface roughness and subsurface damage and their evaluation in fused silica," Opt. Express **26**(4), 4638–4655 (2018).
27. B. Chen, S. C. Li, Z. H. Deng, B. Guo, and Q. L. Zhao, "Grinding marks on ultra-precision grinding spherical and aspheric surfaces," Int. J. of Precis. Eng. and Manuf.-Green Tech. **4**(4), 419–429 (2017).
28. T. Z. Wang, H. N. Liu, C. Y. Wu, J. Cheng, and M. J. Chen, "Three-dimensional modeling and theoretical investigation of grinding marks on the surface in small ball-end diamond wheel grinding," Int. J. Mech. Sci. **173**, 105467 (2020).
29. C. L. He, W. J. Zong, C. X. Xue, and T. Sun, "An accurate 3D surface topography model for single-point diamond turning," Int J Mach Tool Manu **134**, 42–68 (2018).
30. C. L. He and W. J. Zong, "Influence of multifrequency vibration on the optical performance of diamond-turned optics and its elimination method," Appl. Opt. **58**(16), 4241–4249 (2019).
31. S. S. Chen, C. F. Cheung, C. Y. Zhao, and F. H. Zhang, "Simulated and measured surface roughness in high-speed grinding of silicon carbide wafers," Int J Adv Manuf Technol **91**(1-4), 719–730 (2017).
32. A. Beaucamp, P. Simon, P. Charlton, C. King, A. Matsubara, and K. Wegener, "Brittle-ductile transition in shape adaptive grinding (SAG) of SiC aspheric optics," Int J Mach Tool Manu **115**, 29–37 (2017).
33. L. Xu, R. Luo, Z. Yang, T. Zha, and D. Hu, ""Modelling and experimental analysis of surface roughness in spherical grinding," Proceedings of the Institution of Mechanical Engineers," Proc. Inst. Mech. Eng., Part B **228**(6), 856–865 (2014).
34. L. Zhang, J. Xie, R. B. Guo, K. K. Wu, P. Li, and J. H. Zheng, "Precision and mirror micro-grinding of micro-lens array on macro-freeform glass substrate for micro-photovoltaic performances," Int J Adv Manuf Technol **86**(1-4), 87–96 (2016).
35. G. P. Yan and F. Z. Fang, "Fabrication of optical freeform molds using slow tool servo with wheel normal grinding," CIRP Annals **68**(1), 341–344 (2019).
36. J. Xie, Z. J. Deng, J. Y. Liao, N. Li, H. Zhou, and W. X. Ban, "Study on a 5-axis precision and mirror grinding of glass freeform surface without on-machine wheel-profile truing," Int J Mach Tool Manu **109**, 65–73 (2016).
37. B. Guo and Q. L. Zhao, "Wheel normal grinding of hard and brittle materials," Int J Adv Manuf Technol **79**(5-8), 873–880 (2015).
38. S. Lin, Z. H. Jiang, and Y. H. Yin, "Research on arc-shaped wheel wear and error compensation in arc envelope grinding," Int J Adv Manuf Technol **103**(5-8), 1847–1859 (2019).
39. N. Wan, C. Xia, H. Zhao, and S. T. Zhang, "5-axis grinding path generation for free-form surface based on plane instantaneous grinding engagements," Int J Adv Manuf Technol **103**(5-8), 1861–1877 (2019).
40. Q. R. Wang, S. Lin, Z. H. Jiang, Y. H. Yin, and Y. Y. Zhao, "Fewer-axis grinding methodology with simultaneously guaranteeing surface accuracy and grinding force for large optical SiC mirror," Int J Adv Manuf Technol **99**(5-8), 1863–1875 (2018).
41. Y. He and Z. T. Chen, ""Achieving quasi constant machining strip width in five-axis frontal grinding with toroidal tools," Proceedings of the Institution of Mechanical Engineers," Proc. Inst. Mech. Eng., Part B **230**(3), 587–592 (2016).
42. S. S. Chen, C. F. Cheung, F. H. Zhang, and M. Y. Liu, "Optimization of tool path for uniform scallop-height in ultra-precision grinding of free-form surfaces," Nanomanuf. Metrol. **2**(4), 215–224 (2019).
43. S. S. Chen, C. F. Cheung, F. H. Zhang, and C. Y. Zhao, "Three-dimensional modelling and simulation of vibration marks on surface generation in ultra-precision grinding," Precis. Eng. **53**, 221–235 (2018).
44. S. S. Chen, C. F. Cheung, and F. H. Zhang, "An experimental and theoretical analysis of surface generation in ultra-precision grinding of hard and brittle materials," Int J Adv Manuf Technol **97**(5-8), 2715–2729 (2018).
45. M. Y. Liu, C. F. Cheung, X. Feng, C. J. Wang, and Z. C. Cao, "Any-degrees-of-freedom (anyDOF) registration for the characterization of freeform surfaces," Precis. Eng. **62**, 170–180 (2020).